ACS OMEGA

Open Access

http://pubs.acs.org/journal/acsodf

Article

Fabrication of Silver Nanoparticle Loaded into Nanocellulose Derived from Hemp and Poly(vinyl alcohol)-Based Composite as an Electrode for Electrochemical Sensors for Lactate Determination

Rujira Phumma, Wisarttra Phamonpon, Nadnudda Rodthongkum,* and Sarute Ummartyotin*

Cite This: *ACS Omega* 2024, 9, 10371−10379

Read Online

ACCESS | Metrics & More | Article Recommendations

ABSTRACT: Nanocellulose derived from hemp (HNC) with the addition of silver nanoparticles (AgNPs) is utilized for improving the electrochemical sensing performances for lactate detection. Initially, HNC is chemically extracted and purified by using alkali treatment and acid hydrolysis. Then, AgNPs are nucleated in situ by the self-reduction process prior to forming a composite with poly(vinyl alcohol) (PVA). This nanocomposite significantly improves the electrochemical properties of the electrode, including electrochemical conductivity and electrocatalysis. The morphologies and chemical alterations of the HNC/AgNPs-PVA nanocomposite are investigated by field emission scanning electron microscopy. It demonstrates a three-dimensional network with random orientation of the nanocellulose fiber. The AgNPs are well-dispersed in the nanocomposite. Moreover, the nanocomposite provides high thermal stability up to 450 °C. Then, it is remarkably noted that 10 wt % HNC/AgNPs-PVA modified on the electrode provides the highest current responses, with a standard redox couple $[(Fe(CN)_6]^{3-/4-}$. For lactate detection, this modified screen-printed graphene electrode with nonimmobilized lactate oxidase exhibits an increase in the current signal with the increment of lactate concentration and offered a linear range of 0−25 mM, covering a cutoff value (12.5 mM) for muscle fatigue indication. Eventually, this sensor is successfully applied for lactate detection with high potential for a wearable lactate sensor.

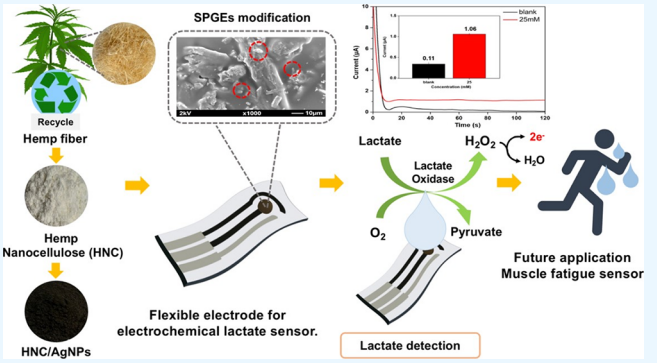

1. INTRODUCTION

With the exponential growth of the worldwide population, various technologies have been extensively developed in order to facilitate the users. The role of numerous technologies has been extremely conducted from research policies based on the guidance of both academia and industry. Although technologies significantly offer numerous advantages including efficiency, productivity, as well as connectivity, they are still limited due to high cost, complicate processing techniques, and emission of hazardous waste, leading to environmental issues and causing pollution to soil, water and air which is difficult to eliminate. One way to use technology with environmental preservation is to design eco-friendly materials. The objective of eco-friendly products is to replace the traditional one with the additional characteristic of ease of degradation and nontoxicity. It can therefore avoid the landfill space issue.

To the best of authors' knowledge, an eco-friendly material is free from toxicity and has high biocompatibility and a fast rate of biodegradation. Eco-friendly materials are therefore developed to employ in numerous sectors such as infrastructure, automotive part, food packaging, as well as medicine. To design the eco-friendly material for various usages, development of a bio-based composite is considered as one of the most effective strategies.[1] It is employed as a reinforcement part in the composite design owing to its superior properties (e.g., stiffness and tensile strength[2]). Among various types of eco-friendly materials, nanocellulose derived from hemp (HNC) is considered one of the most attractive fibers in order to employ as a reinforcement in a biocomposite.[3] Recently, Chen et al.[4] developed cellulose from a hemp-based composite by using the ionic liquid. It offered a high tensile strength and modulus. Mahur et al.[5] studied the role of acid hydrolysis for hemp extraction and purification. The size and percent yield of hemp depend on various ranges of concentration of H_2SO_4. It resulted in high thermal stability when it is employed as a reinforcement in a composite.

Received: October 12, 2023
Revised: November 18, 2023
Accepted: February 8, 2024
Published: February 23, 2024

From the fundamental point of view, hemp (*Cannabis sativa* L.) is one of the oldest crops and has become the dominant eco-friendly fiber in the present. It particularly consists of three main components, which are cellulose (73−95%), hemicelluloses (7−9%), and lignin (4−6%). It significantly provides excellent mechanical properties such as high stiffness, high tensile strength, as well as high solvent resistance.[6] Moreover, it offers high thermal stability and dimensional stability leading to various applications.[7] Furthermore, with the high content of cellulose derived from hemp, it is used in many advanced applications including textiles, pharmaceuticals, health products, plastic composites, and chemical sensors.[7] It can be employed as a degradable medical protective textile. Liu et al.[8] developed a hemp-based composite for a wearable sensor to monitor human activities. From the fundamental point of view, the core technology of a hemp-based material is cellulose. It can be considered as a source for cellulose production. Cellulose is defined as an organic compound with an empirical formula of $(C_6H_{10}O_5)_n$. It is typically related to a polysaccharide consisting of linear chain of β (1 → 4) linked D-glucose units. It is evident that cellulose illustrates high chemical stability and high specific surface area. As a result, it is attractive to design as a platform for electrochemical sensors. It may offer additional characteristics of reliability, speed, as well as accuracy for any diagnostic.

Based on a previous study, the HNC-based composite, as a platform for electrochemical sensors, has been extensively employed as detection platforms, where the electrode configurations are specifically based on either natural or synthetic fabrics.[9] For electrochemical sensors, the screen-printed electrode (SPE) is commonly used due to high effectiveness, portability, low cost, rapid response, good repeatability, as well as flexibility. However, for more utilization, the working electrode (WE) that interacts with the target analyte in the solution can be modified with different modifiers to enhance the electrochemical performance and thus sensibility. Furthermore, it offers a lower detection limit for the trace analysis. With the use of HNC, there are numerous advantages, such as ease of surface modification and high aqueous absorption leading to enhanced sensor performances. Cellulose can be employed as a platform for the chemical synthetic route. Ge et al.[10] developed cellulose aerogel embedded with the ZnO@noble metal for sensitive and reusable SERS application. Wang et al.[11] also developed the carboxymethyl cellulose carbon aerogel and a metal−organic framework for capacitive deionization. N-doping can enhance the conductivity and hydrophilicity.

To enhance the electrical conductivity to the cellulose platform, metal nanoparticles are mostly utilized. Among various types of metal nanoparticles, AgNP is the dominant metal nanoparticle for improving the electrical conductivity of natural fiber because it can be synthesized by means of a green synthetic method through self-reduction using cellulose as a reducing agent.[12] It can offer high level of electrical conductivity while maintaining the uniformity in size and shape along the cellulose network. It is also cheap and eco-friendly. Ettadilin et al.[13] developed the green synthesis of AgNPs onto a cellulose network. It illustrates the excellent electrocatalytic activity for the determination of ornidazole in milk and water.

However, in the case of electrochemical sensors, it gains attention in healthcare applications owing to the fast response, easy fabrication, miniaturized equipment, and quantitative information.[14] It is structurally developed for biorecognition element detection as a biosensor,[15] especially for enzymatic biosensor, by means of measuring H_2O_2. It can be produced from the interaction between a specific enzyme and the target analyte, such as glucose, lactate, and urine.[16] According to the previous study, cellulose from recycled UHT milk carton can be modified and utilized as a novel substrate for both colorimetric and electrochemical lactate sensors for milk spoilage indication. For the electrochemical sensor, aluminum extracted from the milk carton enhanced the current response upon the increase of lactate concentration with a linear range of 0.125−2 M.[17]

Herein, HNC is extracted via alkali treatment and acid hydrolysis. The level of electrical conductivity can be enhanced by the self-reduction method of AgNPs on the fiber network. Then, the modified cellulose with the additional characteristic of electrical conductivity is developed as a nanocomposite hydrogel with poly(vinyl alcohol) (PVA). Then, it is used to modify the WE on the screen-printed graphene electrode (SPGE) to increase the electrochemical sensor performance. Ultimately, it is applied as an electrochemical sensor for sweat lactate detection.

2. MATERIALS AND METHODS

2.1. Chemical Reagents and Materials. Hemp fiber was provided as a gift from a local farm in Thailand. Chemical reagents including sodium hydroxide (NaOH; 98%), hydrogen peroxide (H_2O_2), potassium ferricyanide $K_3[Fe(CN)_6]$, and potassium ferrocyanide $K_4[Fe(CN)_6]$ were purchased from Merck Darmstadt, Germany. Sodium sulfate anhydrous (Na_2SO_4) was obtained from Elago Enterprises Pty, Co., Ltd. PVA with a molecular weight of 100,000 g/mol was purchased from Chem-Supply Pty, Ltd., Australia. Glutaraldehyde solution (25% of concentration) for the synthesis ($C_5H_8O_2$) was obtained from ITW Reagents, S.R.L., Co. Ltd., Germany. Silver nitrate ($AgNO_3$), lactate oxidase (LOx) from *Aerococcus viridans*, sodium DL-lactate, and phosphate buffer (PB, 0.1 M, pH 7.4) were obtained from Sigma-Aldrich (St. Louis, MO, USA). Potassium chloride (KCl) was purchased from Ajax Fine Chem, Co., Ltd. All chemicals were of analytical grade and used as received without further purification.

2.2. Methodology. *2.2.1. HNC Extraction.* Initially, raw hemp fiber is cleaned with DI water before grinding with a nanogrinder machine at room temperature for 800 rpm to reduce the size. After that, the nanocellulose is extracted by boiling with 6 wt % of NaOH at 80 °C with continuous stirring for 4 h. Then, the pretreated nanocellulose is washed by boiling with the mixture solution of 4 wt % of Na_2SO_4 and 5 wt % of H_2O_2 at 80 °C with continuous stirring for 4 h. Afterward, the nanocellulose is washed until neutral pH. Then, it is dried at 70 °C for 24 h and stored in a desiccator in order to avoid moisture absorption.

2.2.2. Self-Reduction Process of AgNPs on HNC. 0.2 M $AgNO_3$ solution is continuously stirred at 60 °C for 1 h in order to ensure the homogeneity, as suggested by the previous report.[18] Then, the solution is poured into the cellulose suspension. The mixture is then continuously stirred for 30 min in order to ensure uniformity. After that, 10 mL of 1 M NaOH solution is slightly dropped into the solution. The mixture is continuously stirred for 30 min. Then, it is centrifuged at 15,000 rpm for 10 min in order to remove the solvent and excess unreacted chemical reagents. Afterward, it is

https://doi.org/10.1021/acsomega.3c08000
ACS Omega 2024, 9, 10371−10379

dried at 70 °C for 24 h to obtain the HNC/AgNP nanocomposite. The sample is kept in a desiccator in order to avoid moisture absorption.

2.2.3. Modification of HNC/AgNPs-PVA Composite on SPGE for Electrochemical Lactate Sensor. The SPGE is prepared by the screen-printing process using Ag/AgCl paste as the reference electrode, while the graphene paste is then employed as the counter electrode and the working electrode. Then, 1, 3, 5, and 10 wt % of HNC/AgNPs is added into 10% v/v glutaraldehyde solution, followed by 5 wt % of PVA. Then, it is continuously stirred at 90 °C for 1 h in order to ensure homogeneity. After that, the HNC/AgNPs-PVA gel solution is obtained before 10 μL of HNC/AgNPs-PVA gel solution by drop-casting on the WE of SPGE. Then, it is dried at room temperature. For lactate detection, the lactate analyte is incubated with LOx (100 unit/mL) in the ratio of 1:20 for 5 min before detection.

2.3. Characterizations. *2.3.1. Scanning Electron Microscopy and Energy-Dispersive X-ray Spectrometry.* The morphological appearance and elemental analysis of the sample are investigated using scanning electron microscopy (SEM) combined with energy-dispersive analysis (EDX) and mapping by FE-SEM (JEOL JSEM7800F, Japan). Prior to investigation, the sample is gold-sputtered for 45 s at 23 mA in order to enhance the conductivity. The magnification of 1000× and an acceleration voltage of 1 kV are employed.

2.3.2. Transmission Electron Microscopy. The microstructures of the sample are characterized by transmission electron microscopy (TEM, JEM-1400, Japan). The magnification is set to be 40,000×. Before analysis, the sample is dispersed into DI water by sonication in order to avoid the agglomeration. Then, it is placed onto a molybdenum grid.

2.3.3. Fourier Transform Infrared Spectroscopy. The functional group of samples is determined by Fourier transform infrared spectroscopy (FTIR, INVNO FTIR Bruker, Germany). The samples are recorded in the wavenumber region of 4000−400 cm $^{-1}$ at a resolution of 4 cm $^{-1}$ and 64 scans.

2.3.4. X-ray Diffraction. The crystallinities of the sample are recorded by X-ray diffraction (XRD, Bruker, D8 Advance). During measurement, CuKα radiation is employed as the X-ray source. The diffraction angle is set from 10 to 80° at a scan rate of 2°/min. Prior to analysis, the sample is dried in order to remove the humidity.

2.3.5. Thermogravimetric Analysis. The thermal decomposition behavior of the sample is investigated by thermogravimetric analysis (TGA, Mettler Toledo, Switzerland). The samples are heated at a heating rate of 10 °C/min under a nitrogen atmosphere from room temperature to 600 °C.

2.3.6. Confocal Laser Scanning Microscopy. The samples are characterized by confocal laser scanning microscopy (CLSM, Olympus/model: LEXT OLS5000) in the profile roughness function to identify the average roughness (R_a) and surface area of the samples. A magnification of 20× is used for the experiment. Each piece of sample is repeated at least in three areas in order to report as a statistical average.

2.4. Electrochemical Measurement. The electrochemical measurement is performed by cyclic voltammetry (CV), electrochemical impedance spectroscopy (EIS), and amperometry by using a Palmsens 4 potentiostat. Initially, CV is used to investigate the current response of the modified SPGE using 5 mM ferri/ferrocyanide $[Fe(CN)_6]^{3-/4-}$ in 0.1 M KCl. The scanning potential is set between −1 and +1 V with a scan rate of 0.1 mV s^{-1}. Then, EIS is performed to observe the electron transfer by inputting a frequency range of 10^{-1}−10^{6} Hz with an amplitude of 100 mV. Then, amperometry is used to determine the lactate concentration in the range of 0−25 mM with a controlled potential of +0.65 V for 120 s. All standard solutions are prepared in 0.1 M PB (pH 7.4), and the experiment is repeated at least thrice ($n \geq 3$) in order to ensure the statistical average.

3. RESULTS AND DISCUSSION

3.1. Physical and Chemical Characterizations of HNC/AgNPs-PVA Composites. HNC/AgNPs-PVA nanocomposites are successfully synthesized as a hydrogel form. They are typically presented in the similar feature compared to pristine PVA. They are easy to stretch and reform when an external load is applied. With the increment of HNC in the hydrogel composite, the dimensional stability of the hydrogel is

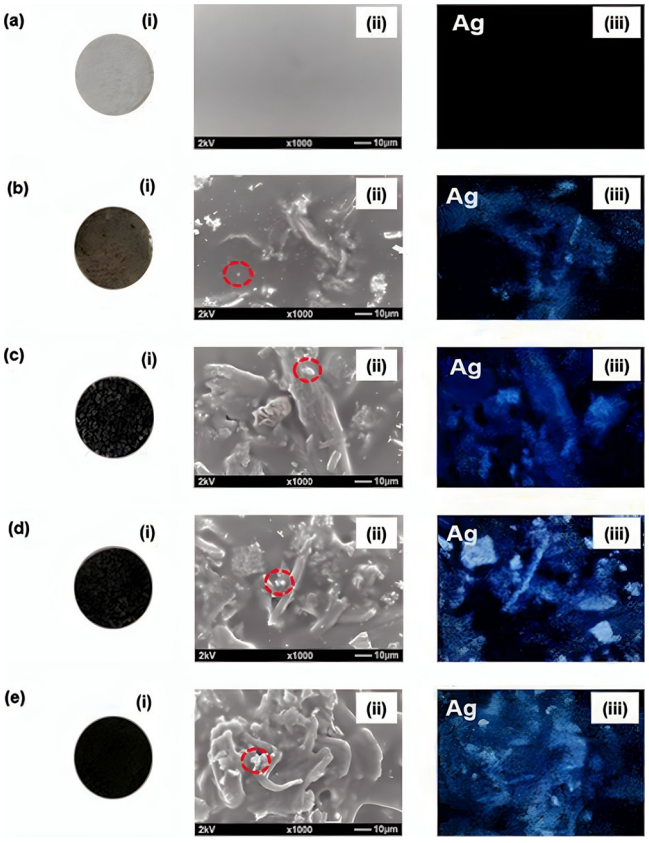

Figure 1. Appearances (i), FE-SEM images (ii), and surface mapping (iii) of unmodified PVA (a), 1 wt % HNC/AgNPs-PVA (b), 3 wt % HNC/AgNPs-PVA (c), 5 wt % HNC/AgNPs-PVA (d), and 10 wt % HNC/AgNPs-PVA (e).

Table 1. SEM-EDX Analysis of HNC/AgNPs-PVA Composites

	elements (wt %)			
sample	C	O	N	Ag
unmodified PVA	63.83	36.17		
1 wt % HNC/AgNPs-PVA	35.59	39.89	4.48	20.04
3 wt % HNC/AgNPs-PVA	35.74	39.04	2.09	23.13
5 wt % HNC/AgNPs-PVA	34.94	32.79	4.36	27.91
10 wt % HNC/AgNPs-PVA	30.91	31.22	5.30	32.58

https://doi.org/10.1021/acsomega.3c08000
ACS Omega 2024, 9, 10371−10379

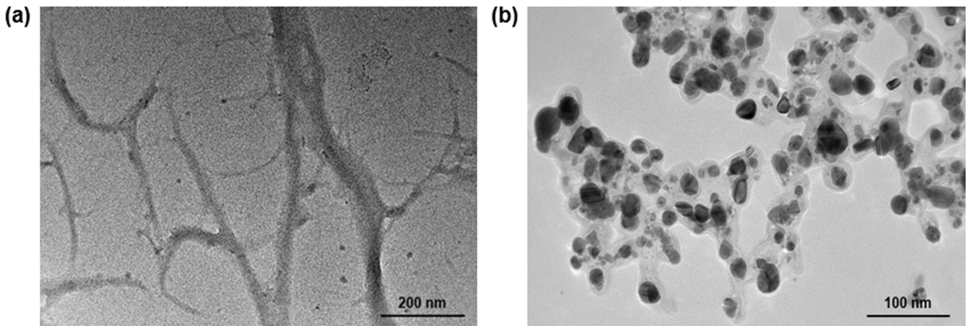

Figure 2. TEM micrographs of HNC/AgNPs-PVA composites. (a) HNC and (b) HNC/AgNPs in magnification of 40,000×.

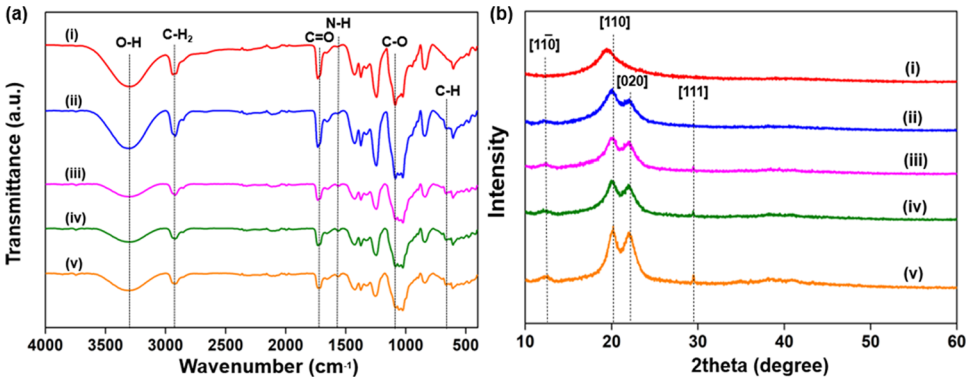

Figure 3. FTIR spectra (a) and XRD patterns (b) of unmodified PVA (i), 1 wt % HNC/AgNPs-PVA (ii), 3 wt % HNC/AgNPs-PVA (iii), 5 wt % HNC/AgNPs-PVA (iv), and 10 wt % HNC/AgNPs-PVA (v).

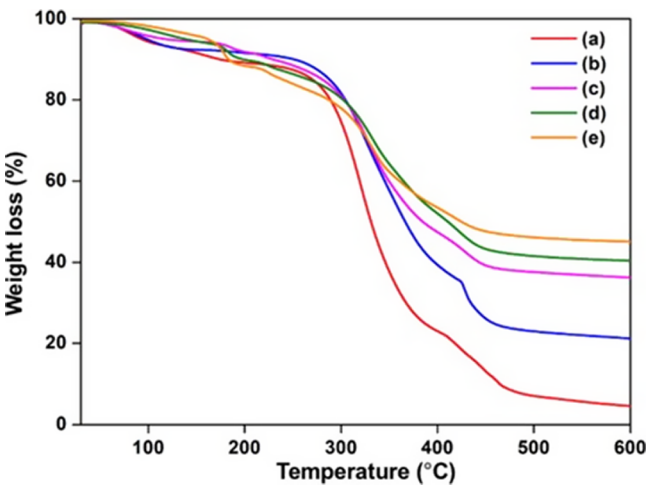

Figure 4. Thermal decomposition behavior of unmodified PVA (a), 1 wt % HNC/AgNPs-PVA (b), 3 wt % HNC/AgNPs-PVA (c), 5 wt % HNC/AgNPs-PVA (d), and 10 wt % HNC/AgNPs-PVA (e).

significantly increased. HNC can form a chemical bonding with PVA throughout the hydrogel network. Furthermore, it is noted that all hydrogels illustrate a high content of water located inside a three-dimensional network of the hydrogel composite. Figure 1i presents the appearance of the hydrogel-based composite. It is observed that with the increment of HNC, the color changes from white to dark gray, as observed in (a)−(e). The roughness on the surface is present due to the existence of AgNPs on the HNC surface. Moreover, Figure 1ii reports the morphological properties of the HNC/AgNPs-PVA composite. It shows the randomly oriented HNC within the PVA network. It is a nonuniformed distribution. PVA solution is filled into the HNC network and then formed the composite. The interface between HNC and PVA is therefore observed. On the other hand, various white spots can be detected on the composite surface. It is noted as a red circle. This spot is typically due to AgNPs. It can be observed that a nonuniform distribution of AgNPs is presented. This is in agreement with the previous article of Madivoli et al.[19]

Figure 1iii reports the mapping analysis allowing to investigate the elemental analysis of AgNPs. The blue color is typically due to the presence of AgNPs. This result can be used to confirm the distribution of white spots in Figure 1ii. Furthermore, it is observed that the intensity of blue color is significantly increased with respect to the amount of HNC. This result is associated with the previous literature of Singh and Mijakovic.[20] This is probably due to the fact that AgNPs are successfully entrapped within the HNC network during the self-reduction process, in which the HNC acted as a reducing agent for AgNP formation with the reduction of Ag^{+} to Ag^{0}, as suggested by Thiagamani et al.[21] Furthermore, the surface area and roughness (R_a) of the sensor platform are analyzed using CLSM. For unmodified electrodes, the R_a values and surface area are 0.544 ± 0.13 and 0.869 ± 0.09 μm, respectively. For modified electrodes, the R_a values and surface area are 15.601 ± 0.12 and 9.329 ± 0.05 μm, respectively. Therefore, it is observed that after modification, the surface area is significantly increased, leading to improved sensitivity.

EDX analysis is carried out to determine the elemental analysis of HNC/AgNPs-PVA composites. As shown in Table 1, compared to unmodified PVA, carbon and oxygen are present. This is in agreement with the previous articles related to pristine PVA.[22−24] Furthermore, in the case of addition of AgNPs into the composite, nitrogen and silver are present. The signal of nitrogen is typically due to the unreacted [NO_3^-]. It

https://doi.org/10.1021/acsomega.3c08000
ACS Omega 2024, 9, 10371−10379

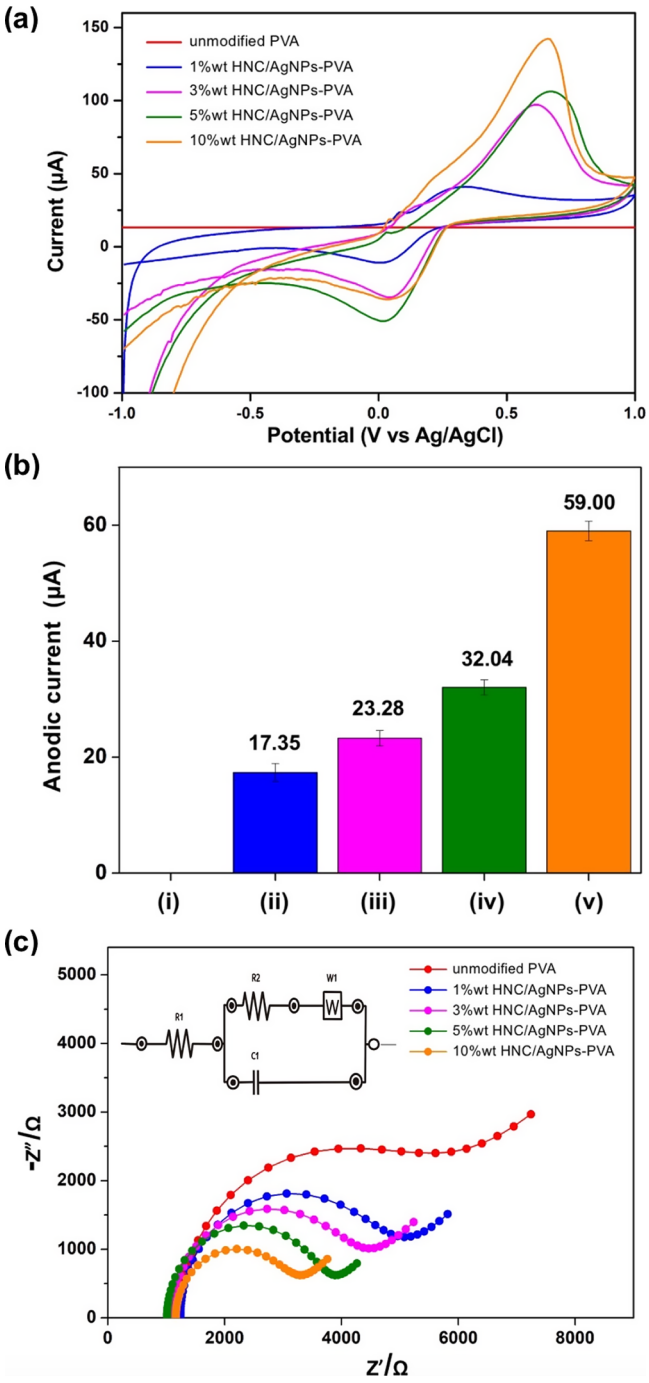

Figure 5. Cyclic voltammogram (a), anodic peak current (b), and Nyquist plots (c) of unmodified PVA (i), 1 wt % HNC/AgNPs-PVA (ii), 3 wt % HNC/AgNPs-PVA (iii), 5 wt % HNC/AgNPs-PVA (iv), and 10 wt % HNC/AgNPs-PVA (v) measuring with 5 mM $[Fe(CN)_6]^{3-/4-}$ by scanning the potential from −1 to 1 V with the scan rate of 0.1 V/s ($n \geq 3$).

is difficult to remove from the dissociation process of silver nitrate. However, the signal of silver is also present in all composites. It is remarkable to note that the percent of silver is slightly increased with respect to the amount of HNC. It can be implied that AgNPs are formed by the self-reduction process onto the HNC network, as suggested by Fouda et al.[25] This result is well corresponded with the mapping analysis as reported in Figure 1.

The morphological properties of HNC and AgNPs formed by self-reduction process onto the HNC network were studied using TEM, as shown in Figure 2. It is observed that the nanoscale size of cellulose fiber is successfully prepared with a randomly oriented network. This is in agreement with the FE-SEM analysis reported in Figure 1ii. In addition, with the increment of magnification, various dark spots are present on the HNC network verifying the existence of AgNPs. It is presented as a spherical shape with various sizes based on the self-reduction process. This may typically relate to nucleation and/or thermodynamic equilibrium, as suggested by Jia et al.[26] Various sizes of the HNC network are present due to the role of carboxyl and hydroxyl groups in the cellulose network. It is to reduce the AgNPs by changing Ag ions into Ag^0 and attaching on the cellulose structure.[27]

In order to determine the functional group of HNC/AgNPs-PVA composites, FTIR spectra is employed. Figure 3a reports the FTIR spectra of HNC/AgNPs-PVA composites. All of the curves are present with identical features. It is similar to pristine PVA. This is probably due to the fact that PVA is the main component in the hydrogel composite. HNC and AgNPs are located inside the PVA network. However, it is observed that the broad region of the characteristic peak at the wavenumber of 3100−3600 cm^{-1} is present. This is typically attributed to O−H stretching. It is because hydroxyl group formation belonged to both HNC and PVA.[28] The presence of this functional group can be used to determine the ability to form hydrogen bonding with the water molecule on the surface. This is in agreement with the contact angle measurement. The characteristic peaks at the wavenumbers of 2940, 1732, 1565, and 1074 cm^{-1} are present, which correspond to the C−H stretching, C═O stretching, N−H stretching, and C−O stretching, respectively.[29−31] These peaks belong to PVA. However, it is observed that the intensity of the peak is slightly reduced when HNC/AgNPs is added into the composite. The existence of AgNPs may be obscure. Furthermore, it is observed that the characteristic peak at the wavenumber of 664 cm^{-1} is present. This is typically related to the vibration of C−H bending caused by the AgNPs, attributed to the metal−ligand frequency stretching, as suggested by previous literature.[32,33]

To determine the crystallinity of HNC/AgNPs-PVA composites, XRD technique is employed. Figure 3b displays the XRD pattern of HNC/AgNPs-PVA composites. The pristine PVA is also provided for comparison. It is observed that all of the characteristic peaks are typically present with the similar feature. It may probably be due to a small portion of HNC and AgNPs. Both of them are mostly integrated inside the PVA network. No significant change related to crystallinity is observed when HNC and AgNPs are integrated. However, it is noted that the intensity is slightly shifted higher when HNC existed. This is similar to the previous result in the literature.[34] It is evident that the diffraction angles of 12.5, 21, and 21.9° are present. These characteristic peaks correspond to the diffraction indices of [1 −1 0], [1 1 0], and [0 2 0], respectively. This is in agreement with the previous works of Gong et al.[35] and Liu et al.[36] It is also typically related to the Miller index of pristine PVA and cellulose.[37] Furthermore, with the existence of AgNPs in the composite, a low intensity of peak is observed at the diffraction angle of 28.9°. It is attributed to the diffraction plane of (111) caused by the presence of AgNPs.[38] With the increase of HNC/AgNPs, the

https://doi.org/10.1021/acsomega.3c08000
ACS Omega 2024, 9, 10371−10379

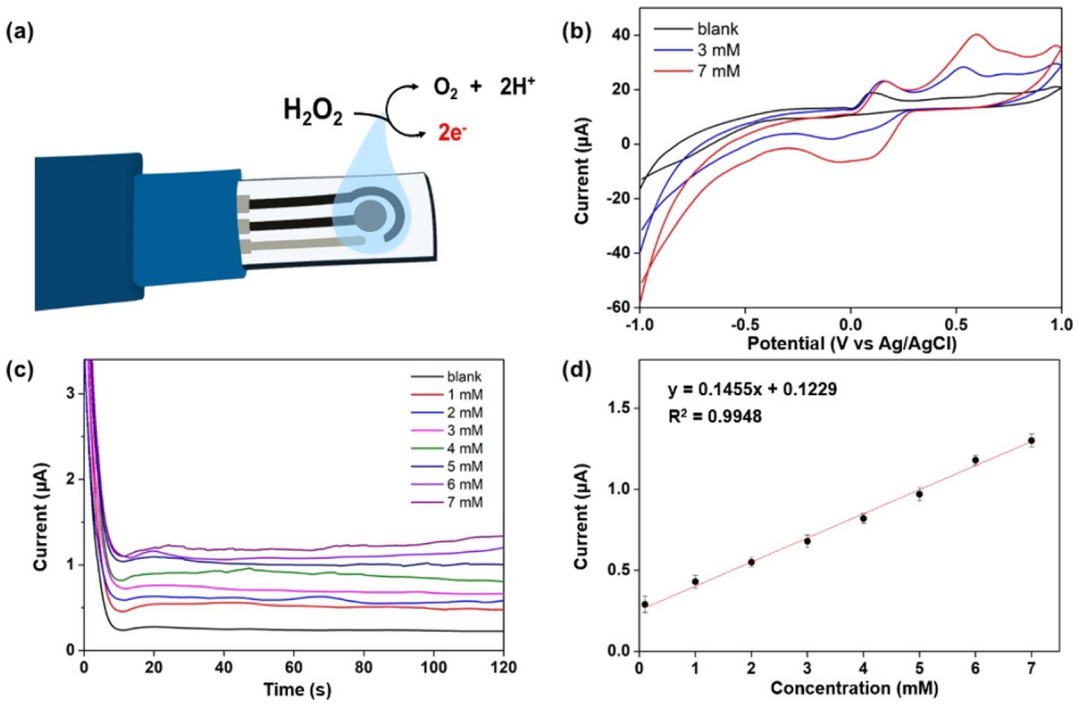

Figure 6. Sensing mechanism of the HNC/AgNPs-PVA composite-modified SPGE for H_2O_2 detection (a). Cyclic voltammogram (b), amperogram (c), and calibration curve (d) of 10 wt % HNC/AgNPs-PVA measuring in 0.1 M PB with 0−7 mM H_2O_2 at an applied potential of +0.65 V for 120 s. The error bars correspond to standard deviation obtained from more than three measurements ($n \geq 3$).

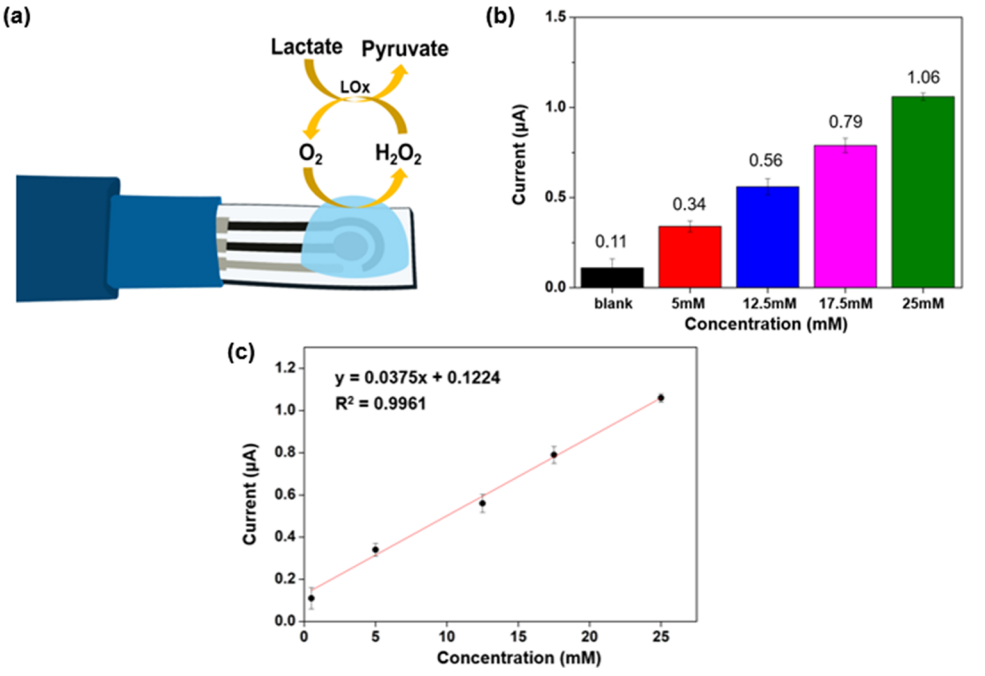

Figure 7. Sensing mechanism of the HNC/AgNPs-PVA composite-modified SPGE for lactate detection (a), current response of lactate in the concentration range of 0−25 mM from amperometry measurements (b), and calibration curve between the lactate concentration and the current response (c). The error bars correspond to standard deviation obtained from more than three measurements ($n \geq 3$).

intensity is therefore slightly high. It could significantly improve the crystallinity of the composite.

To employ the HNC/AgNPs-PVA composites-modified electrode in the electrochemical sensor, the thermal stability of the sample is considered as one of the most important characteristics. In order to predict the thermal stability of the composite, thermal decomposition behavior investigated by TGA is presented. Figure 4 displays the thermal decomposition behavior of HNC/AgNPs-PVA composites. It is observed that the thermal degradation behavior can be classified into three distinct regions based on an applied elevated temperature. From ambient temperature to 300 °C, only 20 wt % of weight loss is presented. This is probably due to solvent and water removal from the hydrogel. This

https://doi.org/10.1021/acsomega.3c08000
ACS Omega 2024, 9, 10371−10379

Table 2. Comparison between Electroanalytical Platform and Our Work[a]

materials	linear range (mM)	LOD (mM)	reference
SPE/PBNcs/GOx	1−24	1.31	46
Au/Pt/Chit/LOx	nonlinear	1.00	47
Au/TTF/CNT/LOx-CS-CNT	1−24		48
CNT/TTF/LOx/Chit	1−20		49
HNC/AgNPs-PVA	0−25	0.56	our work

[a]Abbreviations: HNC, hemp nanocellulose; AuNPs, gold nanoparticles; PVA, poly(vinyl alcohol); BC, bacterial cellulose; SPE, screen-printed electrode; GOx, glucose oxidase; CNT, carbon nanotubes, TTF, tetrathiafulvalene; LOx, lactate oxidase; Chit, chitosan; CNCs, cellulose nanocrystals.

composite can be applied at room temperature without any concern of thermal stability. Then, when the temperature range is elevated to 300−500 °C, a broad region of weight loss is observed. This is due to pyrolysis of HNC and PVA compound. It is changed to volatile gas such as CO_2 and NO_x within this stage. It theoretically involves the exothermic reaction.[39] After that, when the temperature is above 500 °C, percent of weight loss is very low. It can be seen that no pyrolysis occurred. The rest is typically referred to char and residual. This is in agreement with the previous work of Nurazzi et al.[40]

3.2. Electrochemical Characterization of HNC/AgNPs-PVA Nanocomposite Electrode. HNC/AgNPs-PVA composite is successfully prepared as a hydrogel-modified working electrode for the electrochemical sensor. To evaluate the electrochemical properties, CV and EIS are employed. Both techniques are used to evaluate the possibility of composite modification for the WE. Figure 5 demonstrates the electrochemical properties of the HNC/AgNPs-PVA composite by means of cyclic voltammograms, anodic peak current responses, and Nyquist plots. With higher amount of HNC/AgNPs, the redox current is subsequently high in order of magnitude. This is also in agreement with the anodic current response compared to pristine PVA. This is probably due to the fact that with the presence of HNC and AgNPs within the nanocomposite, the specific surface area and electrocatalytic activity are substantially increased, leading to increase in the current response signal. In addition, the AgNPs can catalyze the charge transfer when it is activated, as indicated by Biyoshi et al.[41] It can help to promote the electron transfer between the analyte solution and the sensing area. Moreover, the Nyquist plots obtained from EIS can be used to investigate the electron-transfer efficiency between the electrode and a redox couple $[Fe(CN)6]^{3-/4-}$, related to impedance change via Rct value.[42,43] Figure 5c shows the EIS spectra obtained from unmodified and modified electrodes. The unmodified electrode shows an R_{ct} value of 2.46 kΩ. After modification of electrodes, the Rct value decreases from 2.46 to 1.01 kΩ with higher amount of HNC/AgNPs. Based on the electrochemical characterization results, it can be concluded that 10 wt % HNC/AgNPs-PVA significantly offers the highest current responses and the lowest charge-transfer resistance. Therefore, it can be remarkably noted that it is suitable for electrochemical sensor applications.

To evaluate the applicability of 10 wt % HNC/AgNPs-PVA modified SPGE for the electrochemical lactate sensor, the investigation of electrochemical detection of H_2O_2 is first performed. The presence of H_2O_2 is considered as a byproduct of the reaction between lactate and lactate oxidase, as illustrated in Figure 66a, which presents the sensing mechanism. Furthermore, Figure 6b exhibits the CV and amperometry for the sensing performance in the detection of H_2O_2. The outstanding anodic peak is typically found at +0.65 V, which is related to the current response of H_2O_2, similar to the previous report.[44] Furthermore, with more specific observation, Figure 6c shows the results obtained from the amperometry technique. Different concentrations of H_2O_2 are investigated proportional to the amperometric current response from 0 to 7 mM in 0.1 M PBS at a pH of 7.4 by applying a constant potential of +0.65 V. It is observed that the increment of the current response is attributed to the H_2O_2 concentration. Also, Figure 6d demonstrates the calibration plot for the linearity in the range of 0−7 mM with R^2 of 0.9948, which indicates the superiority of sensing performance for H_2O_2 detection. Thus, this nanocomposite electrode is employed for further application for the enzymatic detection of lactate.

To investigate the applicability of the HNC/AgNPs-PVA nanocomposite electrode for lactate detection, the amperometric detection of lactate is subsequently investigated. Figure 7a shows the sensing mechanism of the HNC/AgNPs-PVA composite-modified SPGE for lactate detection. In addition, Figure 7b displays the amperometric current response for lactate detection. An applied potential of +0.65 V is applied for different concentrations of lactate (0−25 mM). It is tested in 0.1 M PBS (pH 7.4) with the cutoff lactate value of 12.5 mM for muscle fatigue indication.[45] As shown in Figure 7c, the increment of the current response is linearly related to the increase of lactate concentration. Then, a calibration plot of lactate concentration versus the current is plotted with R^2 of 0.9961. Limit of detection (LOD) is calculated by using the equation LOD = $3S_b/m$ where, S_b is the standard of three measurements (n = 3), and m is the slope of calibration LOD of lactate of 0.56 mM.

Table 2 presents the electrochemical properties of the platform between HNC/AgNPs-PVA composite-modified SPGE and many previous literature reports. Our platform presents a similar linear range and LOD. It can be implied that our nanocomposite can be used as a platform for lactate detection.

4. CONCLUSIONS

HNC is successfully extracted from the hemp pulp-based fiber. Then, the nanocomposite between HNC, AgNPs, and PVA is successfully prepared. AgNPs are nucleated by the self-reduction process onto the HNC fiber. The microstructure of the composite is presented as a three-dimensional network, which offers high surface area and thermal stability. The nanocomposite is modified on the working electrode surface to enhance the electrochemical properties toward H_2O_2 and lactate detection. The sensor significantly provides excellent electrochemical performance for enzymatic lactate detection It is verified by the increment of current response with the increase of lactate concentration between 0 and 25 mM. In addition, it covers a cutoff lactate value in human sweat (12.5 mM) for muscle fatigue indication with R^2 of 0.9961 and detection limit of 0.56 mM. Ultimately, this sensor might be an alternative platform for sweat lactate sensor in healthcare applications in the future.

https://doi.org/10.1021/acsomega.3c08000
ACS Omega 2024, 9, 10371−10379

AUTHOR INFORMATION

Corresponding Authors

Nadnudda Rodthongkum − *Metallurgy and Materials Science Research Institute and Center of Excellence in Responsive Wearable Materials, Chulalongkorn University, Bangkok 10330, Thailand;* orcid.org/0000-0002-0379-5166; Email: Nadnudda.r@chula.ac.th

Sarute Ummartyotin − *Department of Materials and Textile Technology, Faculty of Science and Technology, Thammasat University, Pathumthani 12120, Thailand; Center of Excellence on Petrochemical and Materials Technology, Chulalongkorn University, Bangkok 10330, Thailand;* orcid.org/0000-0002-6102-6410; Email: sarute@tu.ac.th

Authors

Rujira Phumma − *Department of Materials and Textile Technology, Faculty of Science and Technology, Thammasat University, Pathumthani 12120, Thailand*

Wisarttra Phamonpon − *Nanoscience and Technology Program, Graduate School, Chulalongkorn University, Bangkok 10330, Thailand*

Complete contact information is available at: https://pubs.acs.org/10.1021/acsomega.3c08000

Notes

The authors declare no competing financial interest.

ACKNOWLEDGMENTS

This work is supported by the Thailand Science Research and Innovation Fundamental Fund fiscal year, 2024. S.U. would like to acknowledge the financial support from Thammasat University Research Unit in Textile and Polymer Chemistry. This research and innovation activity is funded by Hub of Talent: Sustainable Materials for circular economy, National Research Council of Thailand (NRCT). Dr. N.R. would like to acknowledge the financial supported from NSRF via the Program Management Unit for Human Resources & Institutional Development, Research and Innovation (B16F640190).

REFERENCES

(1) Zheng, G.; Kang, X.; Ye, H.; Fan, W.; Sonne, C.; Lam, S. S.; Liew, R. K.; Xia, C.; Shi, Y.; Ge, S. Recent advances in functional utilisation of environmentally friendly and recyclable high-performance green biocomposites: A review. *Chin. Chem. Lett.* **2024**, *35*, No. 108817.

(2) Jawaid, M.; Thariq, M.; Saba, N. *Mechanical and physical testing of biocomposites, fibre-reinforced composites and hybrid composites*; Woodhead Publishing: 2018.

(3) Tanasă, F.; Zănoagă, M.; Teacă, C. A.; Nechifor, M.; Shahzad, A. Modified hemp fibers intended for fiber-reinforced polymer composites used in structural applications—A review. I. Methods of modification. *Polym. Compos.* **2020**, *41* (1), 5−31.

(4) Chen, K.; Xu, W.; Ding, Y.; Xue, P.; Sheng, P.; Qiao, H.; He, J. Hemp-based all-cellulose composites through ionic liquid promoted controllable dissolution and structural control. *Carbohydr. Polym.* **2020**, *235*, No. 116027.

(5) Mahur, B. K.; Ahuja, A.; Singh, S.; Maji, P. K.; Rastogi, V. K. Different nanocellulose morphologies (cellulose nanofibers, nanocrystals and nanospheres) extracted from Sunn hemp (Crotalaria Juncea). *Int. J. Biol. Macromol.* **2023**, *253*, No. 126657.

(6) Karri, R.; Lappalainen, R.; Tomppo, L.; Yadav, R. Bond Quality of Poplar Plywood Reinforced with Hemp Fibers and Lignin-Phenolic Adhesives. *Composites Part C: Open Access* **2022**, *9*, No. 100299.

(7) Promhuad, K.; Srisa, A.; San, H.; Laorenza, Y.; Wongphan, P.; Sodsai, J.; Tansin, K.; Phromphen, P.; Chartvivatpornchai, N.; Ngoenchai, P. Applications of Hemp Polymers and Extracts in Food, Textile and Packaging: A Review. *Polymers* **2022**, *14* (20), 4274.

(8) Liu, Z.; Chen, K.; Fernando, A.; Gao, Y.; Li, G.; Jin, L.; Zhai, H.; Yi, Y.; Xu, L.; Zheng, Y.; Li, H.; Fan, Y.; Li, Y.; Zheng, Z. Permeable graphited hemp fabrics-based, wearing-comfortable pressure sensors for monitoring human activities. *Chemical Engineering Journal* **2021**, *403*, No. 126191.

(9) Sinha, A.; Stavrakis, A. K.; Stojanović, G. M. Textile-based electrochemical sensors and their applications. *Talanta* **2022**, *244*, No. 123425.

(10) Ge, N.; Hu, X.; Pan, Z.; Cai, S.; Fu, F.; Wang, Z.; Yao, J.; Liu, X. Sustainable fabrication of cellulose aerogel embedded with ZnO@noble metal (Ag, Au, Ag-Au) NPs for sensitive and reusable SERS application. *Colloids Surf., A* **2023**, *671*, No. 131650.

(11) Wang, Z.; Gao, M.; Peng, J.; Miao, L.; Chen, W.; Ao, T. Nanoarchitectonics of heteroatom-doped hierarchical porous carbon derived from carboxymethyl cellulose carbon aerogel and metal-organic framework for capacitive deionization. *Int. J. Biol. Macromol.* **2023**, *241*, No. 124596.

(12) Zhang, Y.; Jiang, X.; Zhang, J.; Zhang, H.; Li, Y. Simultaneous voltammetric determination of acetaminophen and isoniazid using MXene modified screen-printed electrode. *Biosens. Bioelectron.* **2019**, *130*, 315−321.

(13) Ettadili, F. E.; Aghris, S.; Laghrib, F.; Farahi, A.; Bakasse, M.; Lahrich, S.; El Mhammedi, M. A. Electrochemical detection of ornidazole in commercial milk and water samples using an electrode based on green synthesis of silver nanoparticles using cellulose separated from Phoenix dactylifera seed. *Int. J. Biol. Macromol.* **2023**, *242*, No. 124995.

(14) Mohankumar, P.; Ajayan, J.; Mohanraj, T.; Yasodharan, R. Recent developments in biosensors for healthcare and biomedical applications: A review. *Measurement* **2021**, *167*, No. 108293.

(15) Vu, Q. K.; Tran, Q. H.; Vu, N. P.; Anh, T.-L.; Le Dang, T. T.; Matteo, T.; Nguyen, T. H. H. A label-free electrochemical biosensor based on screen-printed electrodes modified with gold nanoparticles for quick detection of bacterial pathogens. *Mater. Today Commun.* **2021**, *26*, No. 101726.

(16) Marquette, C. A.; Degiuli, A.; Blum, L. C. J. Electrochemiluminescent biosensors array for the concomitant detection of choline, glucose, glutamate, lactate, lysine and urate. *Biosens. Bioelectron.* **2003**, *19* (5), 433−439.

(17) Phamonpon, W.; Promphet, N.; Ummartyotin, S.; Rodthongkum, N. A dual-lactate sensor for milk spoilage based on modified recycled UHT milk carton cellulose surface. *Journal of Cleaner Production* **2022**, *363*, No. 132519.

(18) Ramakrishna, V.; RimaPaul, M. R.; Ak, M. Effect of NaOH in Polymer Synthesis of Silver Nanoparticles.

(19) Madivoli, E. S.; Kareru, P. G.; Gichuki, J.; Elbagoury, M. M. Cellulose nanofibrils and silver nanoparticles enhances the mechanical and antimicrobial properties of polyvinyl alcohol nanocomposite film. *Sci. Rep.* **2022**, *12* (1), 19005.

(20) Singh, P.; Mijakovic, I. Strong antimicrobial activity of silver nanoparticles obtained by the green synthesis in Viridibacillus sp. extracts. *Frontiers in Microbiology* **2022**, *13*, No. 820048.

(21) Thiagamani, S. M. K.; Rajini, N.; Siengchin, S.; Rajulu, A. V.; Hariram, N.; Ayrilmis, N. Influence of silver nanoparticles on the mechanical, thermal and antimicrobial properties of cellulose-based hybrid nanocomposites. *Compos. B: Eng.* **2019**, *165*, 516−525.

(22) Zhang, K.; Liu, Y.; Shi, X.; Zhang, R.; He, Y.; Zhang, H.; Wang, W. Application of polyvinyl alcohol/chitosan copolymer hydrogels in biomedicine: A review. *Int. J. Biol. Macromol.* **2023**, *242*, No. 125192.

(23) Oun, A. A.; Shin, G. H.; Rhim, J.-W.; Kim, J. T. Recent advances in polyvinyl alcohol-based composite films and their applications in food packaging. *Food Packaging and Shelf Life* **2022**, *34*, No. 100991.

https://doi.org/10.1021/acsomega.3c08000
ACS Omega 2024, 9, 10371−10379

(24) Rivera-Hernández, G.; Antunes-Ricardo, M.; Martínez-Morales, P.; Sánchez, M. L. Polyvinyl alcohol based-drug delivery systems for cancer treatment. *Int. J. Pharm.* **2021**, *600*, No. 120478.
(25) Fouda, M. M.; El-Aassar, M.; El Fawal, G.; Hafez, E. E.; Masry, S. H. D.; Abdel-Megeed, A. k-Carrageenan/poly vinyl pyrollidone/polyethylene glycol/silver nanoparticles film for biomedical application. *Int. J. Biol. Macromol.* **2015**, *74*, 179−184.
(26) Jia, F.; Zhao, D.; Wang, M. Selective nucleation and self-organized crystallization. *Progress in Crystal Growth and Characterization of Materials* **2016**, *62* (2), 252−272.
(27) Cheng, L.; Ren, S.; Lu, X. Application of eco-friendly waterborne polyurethane composite coating incorporated with nano cellulose crystalline and silver nano particles on wood antibacterial board. *Polymers* **2020**, *12* (2), 407.
(28) Abdulkhani, A.; Marvast, E. H.; Ashori, A.; Hamzeh, Y.; Karimi, A. N. Preparation of cellulose/polyvinyl alcohol biocomposite films using 1-n-butyl-3-methylimidazolium chloride. *Int. J. Biol. Macromol.* **2013**, *62*, 379−386.
(29) Ji, Y.; Liang, N.; Xu, J.; Zuo, D.; Chen, D.; Zhang, H. Cellulose and poly (vinyl alcohol) composite gels as separators for quasi-solid-state electric double layer capacitors. *Cellulose* **2019**, *26*, 1055−1065.
(30) Liu, X.; Song, R.; Zhang, W.; Qi, C.; Zhang, S.; Li, J. Development of eco-friendly soy protein isolate films with high mechanical properties through HNTs, PVA, and PTGE synergism effect. *Sci. Rep.* **2017**, *7* (1), 44289.
(31) Zhou, T.; Cheng, X.; Pan, Y.; Li, C.; Gong, L. Mechanical performance and thermal stability of polyvinyl alcohol−cellulose aerogels by freeze drying. *Cellulose* **2019**, *26*, 1747−1755.
(32) Begam, J. N. Biosynthesis and characterization of silver nanoparticles (AgNPs) using marine bacteria against certain human pathogens. *International Journal of Advances in Scientific Research* **2016**, *2* (7), 152−156.
(33) Pinkert, A.; Marsh, K. N.; Pang, S.; Staiger, M. P. Ionic Liquids and Their Interaction with Cellulose. *Chem. Rev.* **2009**, *109* (12), 6712−6728.
(34) Mhlongo, J. T.; Nuapia, Y.; Motsa, M. M.; Mahlangu, T. O.; Etale, A. Green chemistry approaches for extraction of cellulose nanofibers (CNFs): A comparison of mineral and organic acids. *Materials Today: Proceedings* **2022**, *62*, S57−S62.
(35) Gong, J.; Li, J.; Xu, J.; Xiang, Z.; Mo, L. Research on cellulose nanocrystals produced from cellulose sources with various polymorphs. *RSC Adv.* **2017**, *7* (53), 33486−33493.
(36) Liu, P.; Chen, W.; Liu, C.; Tian, M.; Liu, P. A novel poly (vinyl alcohol)/poly (ethylene glycol) scaffold for tissue engineering with a unique bimodal open-celled structure fabricated using supercritical fluid foaming. *Sci. Rep.* **2019**, *9* (1), 9534.
(37) Kumar, A.; Negi, Y. S.; Choudhary, V.; Bhardwaj, N. K. Characterization of cellulose nanocrystals produced by acid-hydrolysis from sugarcane bagasse as agro-waste. *J. Mater. Phys. Chem.* **2014**, *2* (1), 1−8.
(38) Mutiara, T.; Sulistyo, H.; Fahrurrozi, M.; Hidayat, M. Facile route of synthesis of silver nanoparticles templated bacterial cellulose, characterization, and its antibacterial application. *Green Processing and Synthesis* **2022**, *11* (1), 361−372.
(39) Ejara, T. M.; Balakrishnan, S.; Kim, J. C. Nanocomposites of PVA/cellulose nanocrystals: Comparative and stretch drawn properties. *SPE Polymers* **2021**, *2* (4), 288−296.
(40) Nurazzi, N.; Asyraf, M.; Rayung, M.; Norrrahim, M.; Shazleen, S.; Rani, M.; Shafi, A.; Aisyah, H.; Radzi, M.; Sabaruddin, F. Thermogravimetric analysis properties of cellulosic natural fiber polymer composites: A review on influence of chemical treatments. *Polymers* **2021**, *13* (16), 2710.
(41) Bishoyi, A.; Alam, M. A.; Hasan, M. R.; Khanuja, M.; Pilloton, R.; Narang, J. Cyclic voltammetric-paper-based genosensor for detection of the target DNA of Zika virus. *Micromachines* **2022**, *13* (12), 2037.
(42) Yu, Y.; Cheng, Y.; Guo, M.; Li, C.; Hu, J. Ag nanoparticles supported on nickel foam: a flexible 3D electrode for methanol electrocatalytic oxidation. *RSC Adv.* **2017**, *7* (63), 39539−39545.
(43) Khamlich, S.; Khamliche, T.; Dhlamini, M.; Khenfouch, M.; Mothudi, B.; Maaza, M. Rapid microwave-assisted growth of silver nanoparticles on 3D graphene networks for supercapacitor application. *J. Colloid Interface Sci.* **2017**, *493*, 130−137.
(44) Dou, J.; Zhu, G.; Hu, B.; Yang, J.; Ge, Y.; Li, X.; Liu, J. Wall thickness-tunable AgNPs-NCNTs for hydrogen peroxide sensing and oxygen reduction reaction. *Electrochim. Acta* **2019**, *306*, 466−476.
(45) Green, J. M.; Pritchett, R.; Crews, T.; McLester, J.; Tucker, D. Sweat lactate response between males with high and low aerobic fitness. *European journal of applied physiology* **2004**, *91*, 1−6.
(46) Gomes, N. O.; Carrilho, E.; Machado, S. A. S.; Sgobbi, L. F. Bacterial cellulose-based electrochemical sensing platform: A smart material for miniaturized biosensors. *Electrochim. Acta* **2020**, *349*, No. 136341.
(47) Currano, L. J.; Sage, F. C.; Hagedon, M.; Hamilton, L.; Patrone, J.; Gerasopoulos, K. Wearable sensor system for detection of lactate in sweat. *Sci. Rep.* **2018**, *8* (1), 15890.
(48) Payne, M. E.; Zamarayeva, A.; Pister, V. I.; Yamamoto, N. A.; Arias, A. C. Printed, flexible lactate sensors: Design considerations before performing on-body measurements. *Sci. Rep.* **2019**, *9* (1), 13720.
(49) Jia, W.; Bandodkar, A. J.; Valdés-Ramírez, G.; Windmiller, J. R.; Yang, Z.; Ramírez, J.; Chan, G.; Wang, J. Electrochemical tattoo biosensors for real-time noninvasive lactate monitoring in human perspiration. *Analytical chemistry* **2013**, *85* (14), 6553−6560.

https://doi.org/10.1021/acsomega.3c08000
ACS Omega 2024, 9, 10371−10379